CMS Physics Analysis Summary

Contact: cms-pag-conveners-heavyions@cern.ch 2024/10/09

Measurement of the tau $g-2$ factor in ultraperipheral PbPb collisions recorded by the CMS experiment

The CMS Collaboration

Abstract

Measurements of the anomalous magnetic moment of leptons provide stringent tests of the standard model and potential hints of physics beyond the standard model. These measurements for electrons and muons are among the most precisely measured quantities in physics. However, due to the short lifetime of the tau lepton, its anomalous magnetic moment cannot be determined through precession measurements. We report the latest measurement of the anomalous magnetic moment of the tau lepton based on a data sample of ultraperipheral PbPb collisions with an integrated luminosity of up to 1.70 nb^{-1}, depending on the decay channel, collected by the CMS experiment at a center-of-mass energy per nucleon pair of $\sqrt{s_{\text{NN}}} = 5.02$ TeV. The dependence on Z^4 ($Z = 82$ for lead) enhances the cross section for photoproduction with respect to proton-proton and electron-positron collisions. This measurement is improved with respect to the previous CMS measurement via the addition of three tau pair decay modes, a factor of four in luminosity, and the incorporation of both cross section and kinematic distributions in the determination of $g-2$. The measured value of the $\gamma\gamma \to \tau^+\tau^-$ fiducial cross section is the most precise to date, while the $g-2$ measurement is one of the most precise both in PbPb and e^+e^- collisions.

1 Introduction

In numerous, stringent measurements of quantum observables, the standard model (SM) has been remarkably successful in its predictions. For example, the anomalous magnetic moment of the electron ($a_e := (g-2)_e/2$) represents the sum of higher order corrections to that expected from this spin-1/2 particle due to its interaction with electromagnetic, weak, and hadronic fields. The experimental measurement [1] and theoretical calculations [2, 3] of a_e agree to a precision of 10 significant figures, making it the most accurate prediction verified in the history of physics.

Although the SM has been remarkably successful, there are both theoretical and experimental reasons that it cannot be the ultimate fundamental theory of nature. This includes its failure to provide a candidate for the dark matter in the universe. Recently, precise measurements of the anomalous magnetic moment of the muon have shown evidence of deviations from the SM prediction by up to 5.1 standard deviations, depending on the chosen theoretical calculation of the SM prediction [4]. Should a deviation in the anomalous magnetic moment be observed, it would mean that unknown interactions beyond the SM are modifying the expected value. The tau lepton is more sensitive to modifications from the SM to its anomalous magnetic moment (a_τ) due to its larger mass. Given the short lifetime of tau particles, a_τ cannot be measured directly through its precession. The best current measurement of a_τ by the CMS Collaboration [5] is many orders of magnitude less precise than that of the electron and muon. However, most theories of beyond-SM physics expect orders of magnitude larger deviations of the anomalous magnetic moment for tau leptons than for electrons and muons. This motivates methods to improve the a_τ measurement, as presented here.

The measurement of a_τ from photo-produced tau-lepton pairs benefits from the factor of Z^4 cross section enhancement in PbPb interactions ($Z = 82$ for Pb ions) as compared to proton-proton or electron-positron collisions. Photoproduction is prominent in ultraperipheral collisions (UPCs), which occur when the impact parameter of the passing Pb ions is larger than twice their radius. Figure 1 shows the Feynman diagram of PbPb $\to$ Pb$^{(\star)}(\gamma\gamma \to \tau^+\tau^-)Pb^{(\star)}$, in which quasireal photons ($q^2 \to 0$) emitted from the Pb ions produce a pair of almost back-to-back tau leptons. Variations of a_τ in the $\gamma\tau^+\tau^-$ vertices modify both the rate of ditau production and the kinematics of the tau leptons, and can therefore be used to constrain a_τ.

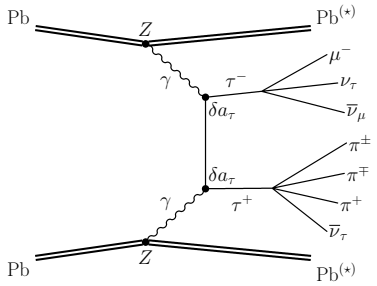

Figure 1: Feynman diagram of the PbPb $\to$ Pb$^{(\star)}(\gamma\gamma \to \tau^+\tau^-)Pb^{(\star)}$. The star in Pb* indicates the possible excitation of the lead ion.

The first observation of this process [6] by CMS was achieved using a $0.4\,\text{nb}^{-1}$ dataset of PbPb collisions at the center-of-mass energy of 5.02 TeV per nucleon recorded in 2015, and in the decay channel shown in Fig. 1, and its charge conjugate, referred to as μ+3prong, in which "prong" refers to the charged pions in the hadronic tau-lepton decay. The analysis presented

here also includes additional $\tau^+\tau^-$ decay modes with final states of μ+1prong, e+3prong, and μ+e, and utilizes the 2018 dataset with an integrated luminosity of 1.61 nb^{-1} for the μ+1prong channel and 1.70 nb^{-1} for the other three channels.

The structure of this note is as follows. After a short description of the CMS experiment in Section 2, background processes and their modeling are discussed in Section 3. Event selection criteria to efficiently reject these backgrounds and target signal events are discussed in Section 4. Finally, signal extraction and limits on the signal cross section and a_τ are discussed in Section 5.

2 The CMS experiment

The CMS apparatus [7] is a multipurpose, nearly hermetic detector, designed to trigger on [8, 9] and identify electrons, photons, muons, τ leptons, jets, and missing p_T [10–12]. A global reconstruction "particle-flow" algorithm [13] combines the information provided by the all-silicon inner tracker, the crystal electromagnetic calorimeter, and the brass and scintillator hadron calorimeter, operating inside a 3.8 T superconducting solenoid, with data from gas-ionization muon detectors embedded in the flux-return yoke outside the solenoid, to build τ lepton candidates and jets, and to measure the missing p_T [14–16]. Forward hadron (HF) calorimeters [17], made of steel and quartz-fibers, extend the $|\eta|$ coverage from 3.0, provided by the barrel and endcap detectors, to 5.2. The HF calorimeters are segmented to form $\Delta\eta \times \Delta\phi$ "towers" of width 0.175×0.175, with ϕ being the azimuthal angle. Two zero degree calorimeters (ZDC), made of quartz fibers and plates embedded in tungsten absorbers, are used to detect neutrons from nuclear dissociation events in the range $|\eta| > 8.3$. Events are selected online using a two-tiered trigger system. The first level, composed of custom hardware processors, uses information from the calorimeters and muon detectors [8]. The second level, known as the high-level trigger [9], consists of a farm of processors running a version of the full event reconstruction software.

3 Backgrounds

Photoproduction in UPC events is distinguished from nuclear interactions by the low number of measured tracks and no activity above noise level in the forward detectors. The Pb ions most often stay intact, although Pb ions excited by the exchange of additional photons may emit neutrons in the forward region instrumented by the ZDC. If the noise level in the detector increases, rejection of non-exclusive photo-produced backgrounds becomes less efficient, leading to one of the main sources of background in this analysis.

In the μ+1prong, μ+3prong, and e+3prong decay modes, the non-exclusive background is modeled by a data-based "ABCD" method, in which two uncorrelated observables define four regions of phase space, in order to predict the background expected in one region based on a scaling from the other three. Four regions of the phase space are defined with a low or high number of tracks and low or high activity in the HF detector. The background distributions in the signal region with a low number of tracks and low HF activity are estimated bin-by-bin from distributions in the control regions.

Exclusive photoproduction of electron and muon pairs is also considered as a source of background. As with the $\tau^+\tau^-$ signal, the two leptons are produced from two quasireal photons emitted from the Pb ions. Since these photons have a negligible transverse momentum (p_T) of below 30 MeV in LHC conditions, the pair of muons are expected to be back-to-back in the

transverse plane with a total p_T below 60 MeV, making them easy to reject using the selections described in Section 4, given that the presence of neutrinos in the decay of taus generates a likely imbalance of charged decay products. However, final-state-radiation (FSR) from one of the muons generates an imbalance, and therefore the $\gamma\gamma \to \mu^+\mu^-\gamma$ process is a considerable source of background in the μ+1prong channel. This is because a muon without enough transverse momentum to reach the muon chambers is reconstructed as a charged pion. Additionally, a small contribution from the $\gamma\gamma \to e^+e^-$ process is expected in the e+3prong channel, in the case of bremsstrahlung radiation of the electron when interacting with the detector material, generating an additional pair of tracks.

4 Signal selection

Events are selected online by requiring a single muon for the three channels with a muon in the final state and an electron for the e+3prong decay channel. Offline, events are selected to have exactly the number of muons, electrons, and charged pions expected for each decay channel, each having a "high-purity" [12] track, and all within the acceptance of the CMS detector. Muons are required to pass "soft" quality [11] criteria and have a p_T above 3.5 GeV for $|\eta| < 1.2$ or 1.5 GeV for $1.2 < |\eta| < 2.4$. These thresholds are set based on the geometrical acceptance of the CMS muon system. The electron p_T is required to be above 2.5 GeV in the μ+e channel to reduce backgrounds due to electromagnetic calorimeter noise and above 4 GeV in the e+3prong channel due to a higher electron p_T threshold of the online selection. The minimum p_T of the charged pion in the μ+1prong channel is 0.3 GeV. The minimum leading, second leading, and third leading p_T of the three charged pions in the μ+3prong and e+3prong channels is 0.5, 0.3, and 0.3 GeV, respectively. The visible hadronic tau decay in the 3-prong final states is reconstructed from a vector sum of the three charged pions, and its transverse momentum is required to be above 1 GeV in the e+3prong channel, with an invariant mass below 1.5 GeV in both the e+3prong and μ+3prong channels.

Photoproduction of the events is ensured by vetoing events with calorimeter activity above certain thresholds, which reject 99% of the detector noise. In particular, events with an HF tower with energy above 6 GeV are rejected in all decay modes. To further reject photonuclear events in the μ+1prong channel, events with activity above the noise level in any of the two ZDC are rejected. The efficiency of this selection is estimated from the probability of neutron emission in $\mathrm{PbPb} \to \mathrm{Pb}^{(\star)}(\gamma\gamma \to \mu^+\mu^-)\mathrm{Pb}^{(\star)}$ events with the same event selection as the signal, by measuring the number of neutrons on each side of ZDC as a function of the dimuon invariant mass. These probabilities are then applied as weights to the events generated from Monte Carlo simulations as a function of ditau or dimuon invariant mass. Figure 2 shows the probability of having no neutron activity on either side of the ZDC (0n0n), activity on only one side (0nXn), and activity on both sides (XnXn) as a function of the dimuon invariant mass for events satisfying the exclusive photoproduction criteria. The use of the ZDC information in the μ+1prong channel limits the dataset to the events with functional ZDC detectors, lowering the integrated luminosity to 1.61 nb^{-1} for this channel.

To reject non-exclusive events in channels with hadronic tau decays, the acoplanarity of the lepton and the visible reconstructed hadronic tau should be below 0.1. In the μ+e channel, the exclusive dimuon background becomes negligible by requiring the acoplanarity of the two tracks to be above 0.01. In the μ+1prong channel, by requiring the vector sum of p_T of the two tracks to be above 1 GeV, the $\gamma\gamma \to \mu^+\mu^-$ background becomes negligible, and $\gamma\gamma \to \mu^+\mu^-\gamma$ is highly suppressed.

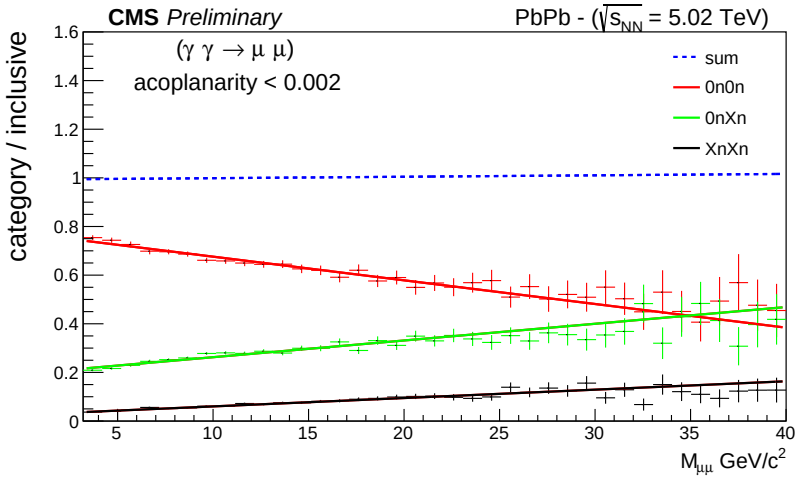

Figure 2: Neutron emission probability as a function of the dimuon invariant mass for each category of neutron emission.

The exclusive $\gamma\gamma \to \mu^+\mu^-\gamma$ background present in μ+1prong and μ+e channels is simulated at leading order with gamma-UPC [18], while the PbPb $\to$ Pb$^{(\star)}(\gamma\gamma \to \tau^+\tau^-)Pb^{(\star)}$ signal is generated at leading order with gamma-UPC using the standard model value of a_τ, and with Upcgen [19] for a_τ values between -0.1 and 0.1, in the fiducial phase space of tau $p_{\mathrm{T}} < 1\,\mathrm{GeV}$ and tau $|\eta| < 3$. These two generators show a good kinematic agreement in tau lepton kinematics when using the same a_τ value and photon flux form factor, with a less than 4% shape variation. The $\gamma\gamma \to \mathrm{e}^+\mathrm{e}^-$ process is simulated using SuperChic [20]. The hadronization and decay of tau leptons are performed using PYTHIA8 (v2.1.2) [21], and GEANT4 [22] is used to emulate the full CMS detector response.

Migration between reconstructed $\tau^+\tau^-$ decay modes may occur, and is maximal in the μ+1prong category which consists of 67.6% real μ+1prong decays and 28% fully leptonic decays. The cross section of the $\gamma\gamma \to \mu^+\mu^-\gamma$ sample is adjusted to the value obtained in a control region in which the vector sum p_{T} of the photon and the two tracks is close to zero.

To ensure that the excess of the observed data over the background is kinematically compatible with the signal, kinematic distributions in each channel are investigated. In all distributions, it is observed that the simulated signal distribution stacked on top of the background model consisting of the data-driven ABCD background, the simulated $\gamma\gamma \to \mu^+\mu^-\gamma$ exclusive background, and/or the $\gamma\gamma \to \mathrm{e}^+\mathrm{e}^-$ exclusive backgrounds is in agreement with data, as seen in Fig. 3 for the lepton p_{T} distributions, which were determined to provide the most sensitivity to a_τ variations.

The main sources of uncertainty in the signal efficiency can be presented as a percentage variation on the cross section measurement at $a_\tau = 0$. These are the understanding of the muon trigger and reconstruction efficiency (2.7%), tracking efficiency of pions (2.0%), measurement of the integrated luminosity (1.5%), choice of specific ABCD regions (1.4%), as well as sub-percent level contributions from the limited MC size, tau branching ratio, electron reconstruction efficiency, efficiency of exclusivity requirements, and the efficiency of the neutron multiplicity categorization.

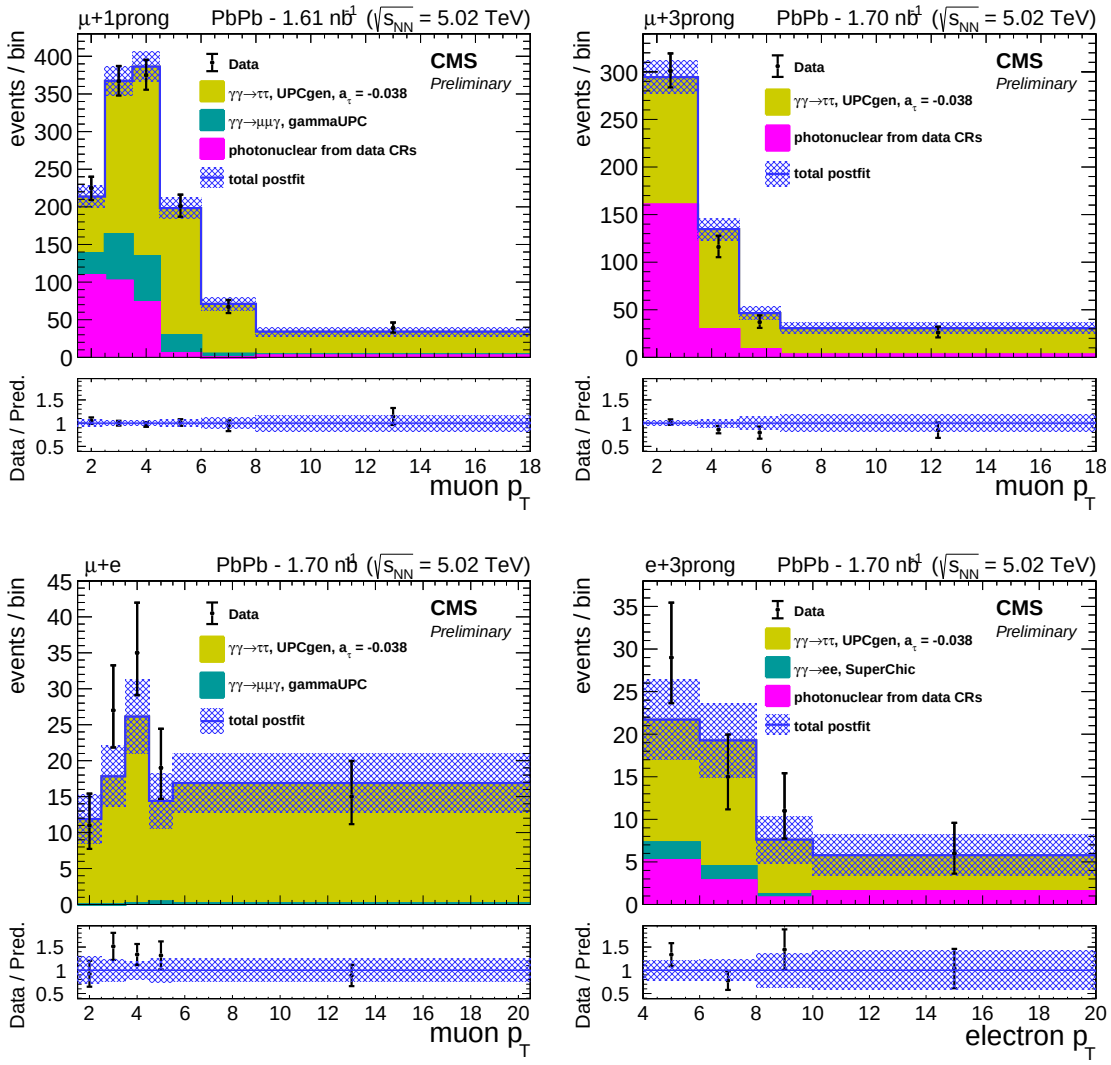

Figure 3: Postfit distributions of lepton p_{T} for the μ+1prong (upper left), μ+3prong (upper right), μ+e (lower left), and e+3prong (lower right) channels. Signal distributions are stacked on top of the background model, consisting of $\gamma\gamma \to \mu^+\mu^-\gamma$, $\gamma\gamma \to \mathrm{e}^+\mathrm{e}^-$, and/or the inclusive background predicted by the ABCD method. The stacked distributions are compared with data (black points).

5 Results

As both the cross section of the signal process and kinematics of the decay products of the tau lepton are sensitive to a_τ, the four lepton p_{T} distributions in Fig. 3 are used to measure a_τ and the cross section in the fiducial phase space defined by tau $p_{\mathrm{T}} > 1\,\mathrm{GeV}$ and tau $|\eta| < 3$. Signal templates are smoothed, and then morphed between the 21 signal samples generated for $-0.1 < a_\tau < 0.1$ to provide finer granularity. The negative log likelihood of the fit of the distribution of signal plus background to data is calculated in a range of a_τ values and fiducial cross sections as shown in the upper plot of Fig. 4, while allowing for variation of the systematic uncertainties. Black 2D contours mark $1\,\sigma$ and $2\,\sigma$ limits on a_τ and the cross section. The degeneracy in a_τ arises because both negative and positive a_τ variations lead to an increase in events in the tail of the lepton p_{T} distribution. This degeneracy is broken by simultaneously measuring the total cross section, which increases monotonically as a_τ increases. The black

dashed line shows the variations of the cross section as a function of a_τ, obtained from UPCgen and normalized to the measured cross section at $a_\tau = 0$. The negative log likelihood variation along this line, as shown in the middle and right plot, is used to set limits on both a_τ and the cross section simultaneously. The effect of the systematic uncertainties, as shown by the difference between the dashed blue and solid black lines, is mainly due to the uncertainties in the muon and pion reconstruction efficiencies, with a smaller effect from the luminosity uncertainty.

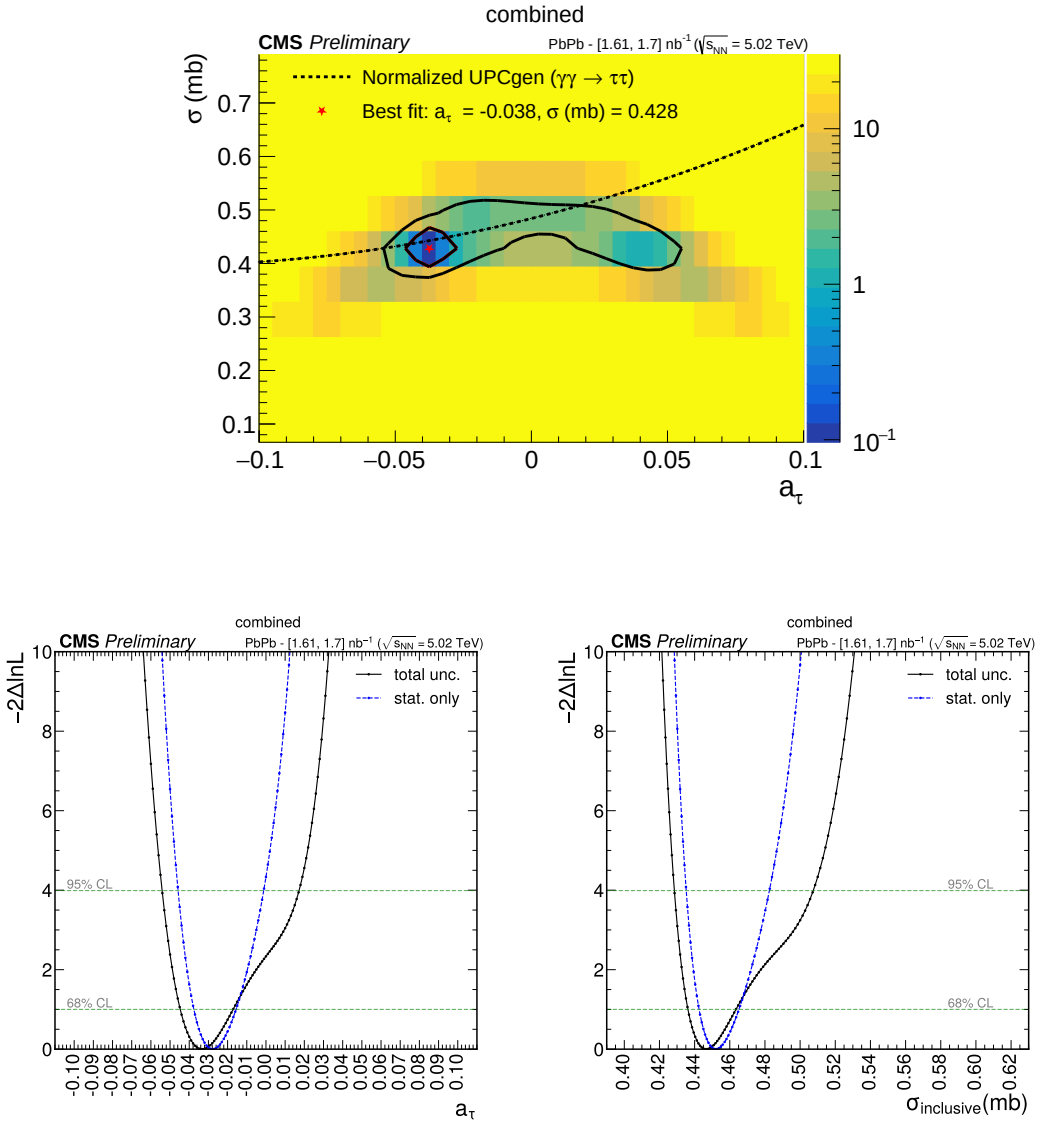

Figure 4: Left: Simultaneous limits on cross section of PbPb $\to$ Pb$^{(\star)}(\gamma\gamma \to \tau^+\tau^-)Pb^{(\star)}$ and a_τ, using the sensitivity of lepton p_T to a_τ. Middle and right: Limits on the signal cross section and a_τ, using the sensitivity of both cross section and lepton p_T to a_τ.

Figure 5 shows a breakdown of the a_τ measurements for each individual channel and combined, compared to a set of previous best measurements. The current best limits on a_τ are obtained by measuring photoproduction of τ lepton pairs in proton-proton collisions recorded by the CMS experiment that makes use of tau pairs with a higher invariant mass, yielding a greater sensitivity to effects from a higher mass scale. This measurement of $a_\tau = -35^{+18}_{-10}\,(\text{stat+sys}) \times 10^{-3}$ provides similar sensitivity and compatible results with those from ATLAS and DELPHI,

and more than a factor of four improvement over the previous CMS measurement using PbPb collisions.

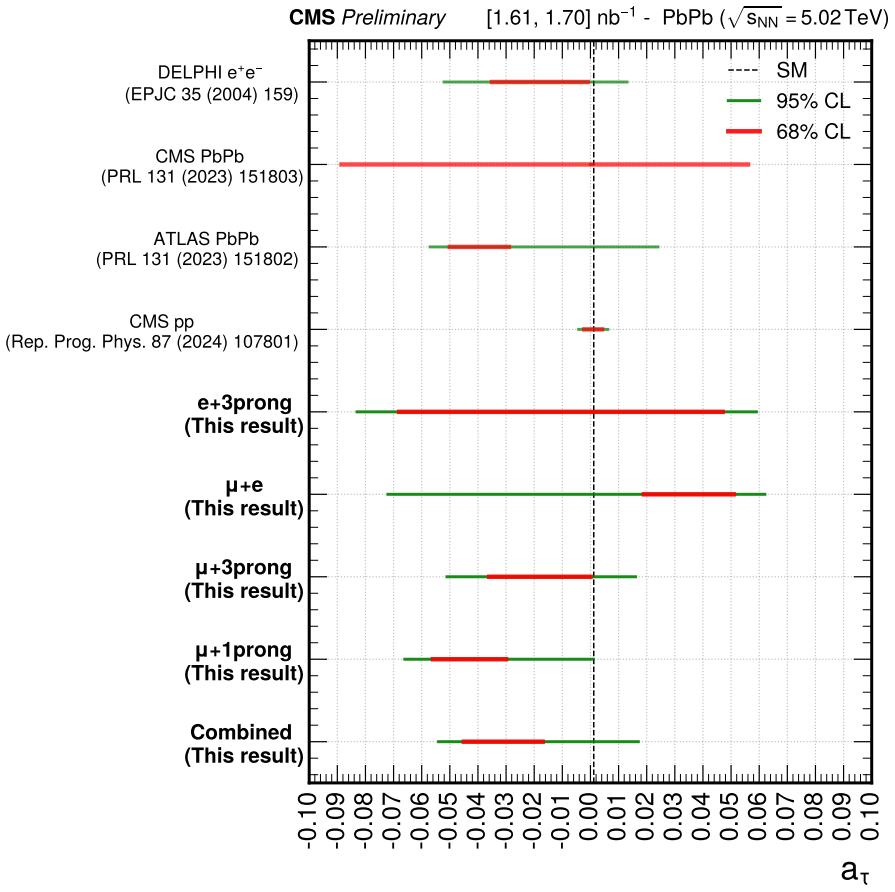

Figure 5: Breakdown of the 68% and 95% limits on a_τ in the four considered decay channels and the combined result, compared to a set of best previous measurements.

Moreover, this study provides the best measurement of the $\gamma\gamma \to \tau^+\tau^-$ cross section, with $\sigma(\gamma\gamma \to \tau^+\tau^-) = 447^{+16}_{-11}$ (stat+sys) μb. The fiducial phase space used in this analysis is significantly larger than the one from the previous CMS measurement [6] with the same colliding system. Given the higher signal efficiency in this study due to more relaxed kinematic requirements, a larger fiducial phase space is needed to fully contain the signal events passing these kinematic requirements.

6 Summary

We report the best measurement of the $\gamma\gamma \to \tau^+\tau^-$ fiducial cross section, $\sigma(\gamma\gamma \to \tau^+\tau^-) = 447^{+16}_{-11}$ (stat+sys) μb, using a data sample of PbPb collisions at a center-of-mass energy per nucleon pair of $\sqrt{s_{\mathrm{NN}}} = 5.02$ TeV. The precision is partly made possible by the high signal efficiency obtained with relaxed requirements on the transverse momenta of the visible decay products of the tau lepton with respect to other measurements. We also report a measurement of $a_\tau = -35^{+18}_{-10}$ (stat+sys) $\times 10^{-3}$. This result represents more than a factor of four decrease in uncertainty on the limits of a_τ as compared to the previous CMS measurement with the same colliding system. This is due to a factor of four increase in luminosity, the inclusion of

the μ+1prong, e+3prong, and μ+e tau-tau decay modes, as well as a more sophisticated likelihood extraction using both the visible τ lepton kinematics as well as the $\tau^+\tau^-$ cross section. The measurement is made in a complementary phase space of $\tau^+\tau^-$ invariant mass as compared to the CMS measurement in proton-proton collisions [5], is compatible with previous measurements, and is of similar sensitivity to the best measurements from ATLAS [23] and DELPHI [24].

References

[1] X. Fan, T. G. Myers, B. A. D. Sukra, and G. Gabrielse, "Measurement of the electron magnetic moment", *Phys. Rev. Lett.* **130** (2023) 071801, doi:10.1103/PhysRevLett.130.071801.

[2] T. Aoyama, M. Hayakawa, T. Kinoshita, and M. Nio, "Tenth-order QED contribution to the electron $g-2$ and an improved value of the fine structure constant", *Phys. Rev. Lett.* **109** (2012) 111807, doi:10.1103/PhysRevLett.109.111807, arXiv:1205.5368.

[3] T. Aoyama, M. Hayakawa, T. Kinoshita, and M. Nio, "Tenth-order electron anomalous magnetic moment — contribution of diagrams without closed lepton loops", *Phys. Rev. D* **91** (2015), no. 3, 033006, doi:10.1103/PhysRevD.91.033006, 10.1103/PhysRevD.96.019901, arXiv:1412.8284. [Erratum: Phys. Rev. D96, no.1, 019901 (2017)].

[4] The Muon $g-2$ Collaboration, "Measurement of the positive muon anomalous magnetic moment to 0.20 ppm", *Phys. Rev. Lett.* **131** (2023) 161802, doi:10.1103/PhysRevLett.131.161802.

[5] CMS Collaboration, "Observation of $\gamma\gamma \to \tau\tau$ in proton-proton collisions and limits on the anomalous electromagnetic moments of the τ lepton", *Reports on Progress in Physics* **87** (2024) 107801, doi:10.1088/1361-6633/ad6fcb.

[6] CMS Collaboration, "Observation of τ lepton pair production in ultraperipheral Pb-Pb collisions at $\sqrt{s_{NN}} = 5.02$ TeV", *Phys. Rev. Lett.* **131** (2023) 151803, doi:10.1103/PhysRevLett.131.151803.

[7] CMS Collaboration, "The CMS experiment at the CERN LHC", *JINST* **3** (2008) S08004, doi:10.1088/1748-0221/3/08/S08004.

[8] CMS Collaboration, "Performance of the CMS level-1 trigger in proton-proton collisions at $\sqrt{s} = 13$ TeV", *JINST* **15** (2020) P10017, doi:10.1088/1748-0221/15/10/P10017, arXiv:2006.10165.

[9] CMS Collaboration, "The CMS trigger system", *JINST* **12** (2017) P01020, doi:10.1088/1748-0221/12/01/P01020, arXiv:1609.02366.

[10] CMS Collaboration, "Electron and photon reconstruction and identification with the CMS experiment at the CERN LHC", *JINST* **16** (2021) P05014, doi:10.1088/1748-0221/16/05/P05014, arXiv:2012.06888.

[11] CMS Collaboration, "Performance of the CMS muon detector and muon reconstruction with proton-proton collisions at $\sqrt{s} = 13$ TeV", *JINST* **13** (2018) P06015, doi:10.1088/1748-0221/13/06/P06015, arXiv:1804.04528.

[12] CMS Collaboration, "Description and performance of track and primary-vertex reconstruction with the CMS tracker", *JINST* **9** (2014) P10009, doi:10.1088/1748-0221/9/10/P10009, arXiv:1405.6569.

[13] CMS Collaboration, "Particle-flow reconstruction and global event description with the CMS detector", *JINST* **12** (2017) P10003, doi:10.1088/1748-0221/12/10/P10003, arXiv:1706.04965.

[14] CMS Collaboration, "Performance of reconstruction and identification of τ leptons decaying to hadrons and ν_τ in pp collisions at $\sqrt{s} = 13\,\text{TeV}$", *JINST* **13** (2018) P10005, doi:10.1088/1748-0221/13/10/P10005, arXiv:1809.02816.

[15] CMS Collaboration, "Jet energy scale and resolution in the CMS experiment in pp collisions at 8 TeV", *JINST* **12** (2017) P02014, doi:10.1088/1748-0221/12/02/P02014, arXiv:1607.03663.

[16] CMS Collaboration, "Performance of missing transverse momentum reconstruction in proton-proton collisions at $\sqrt{s} = 13\,\text{TeV}$ using the CMS detector", *JINST* **14** (2019) P07004, doi:10.1088/1748-0221/14/07/P07004, arXiv:1903.06078.

[17] CMS Collaboration, "Calibration of the CMS hadron calorimeters using proton-proton collision data at $\sqrt{s} = 13\,\text{TeV}$", *JINST* **15** (2020) P05002, doi:10.1088/1748-0221/15/05/P05002, arXiv:1910.00079.

[18] H.-S. Shao and D. d'Enterria, "gamma-UPC: automated generation of exclusive photon-photon processes in ultraperipheral proton and nuclear collisions with varying form factors", *JHEP* **09** (2022) 248, doi:10.1007/JHEP09(2022)248, arXiv:2207.03012.

[19] N. Burmasov, E. Kryshen, P. Bühler, and R. Lavicka, "Upcgen: A Monte Carlo simulation program for dilepton pair production in ultra-peripheral collisions of heavy ions", *Computer Physics Communications* **277** (2022) 108388, doi:https://doi.org/10.1016/j.cpc.2022.108388.

[20] L. Harland-Lang, V. Khoze, and M. Ryskin, "Exclusive LHC physics with heavy ions: SuperChic 3", *Eur. Phys. J. C* **79** (2019) 39, doi:10.1140/epjc/s10052-018-6530-5, arXiv:1810.06567.

[21] T. Sjöstrand et al., "An introduction to PYTHIA 8.2", *Comput. Phys. Commun.* **191** (2015) 159, doi:10.1016/j.cpc.2015.01.024, arXiv:1410.3012.

[22] GEANT4 Collaboration, "GEANT4—a simulation toolkit", *Nucl. Instrum. Meth. A* **506** (2003) 250, doi:10.1016/S0168-9002(03)01368-8.

[23] ATLAS Collaboration, "Observation of the $\gamma\gamma \to \tau\tau$ process in Pb + Pb collisions and constraints on the τ-lepton anomalous magnetic moment with the ATLAS detector", *Phys. Rev. Lett.* **131** (2023) 151802, doi:10.1103/PhysRevLett.131.151802.

[24] DELPHI Collaboration, "Study of tau-pair production in photon-photon collisions at LEP and limits on the anomalous electromagnetic moments of the tau lepton", *Eur. Phys. J. C* **35** (2004) 159, doi:10.1140/epjc/s2004-01852-y, arXiv:hep-ex/0406010.